

Active sites in sol–gel prepared silica-alumina for photoinduced non-oxidative methane coupling

Hisao Yoshida,* Norimitsu Matsushita, Yuko Kato and Tadashi Hattori

Department of Applied Chemistry, Graduate School of Engineering, Nagoya University, Nagoya, 464-8603, Japan. E-mail: yoshidah@apchem.nagoya-u.ac.jp; Fax: +81 52 789 3193

Received 6th December 2001, Accepted 12th February 2002

First published as an Advance Article on the web 22nd April 2002

The photoinduced non-oxidative methane coupling at room temperature was examined by using a series of silica-alumina samples prepared by a sol–gel method, in order to clarify the photoactive sites of silica-alumina. The maximum yield of ethane, the main product in this reaction condition, was obtained on the sample containing around 20 mol% of Al. The variation of ethane yield was consistent with the variation of UV-absorption intensity. Ethene as the minor product, which is obtained by thermal desorption after photoreaction, was produced on the samples of larger Al content. The aluminium sites in the low Al content samples exhibited higher specific activity and higher ethane selectivity than those in high Al content samples. The silica-alumina sample was characterized by using N₂-adsorption, XRD, XPS and Al K-edge XANES. In addition to UV spectroscopy, phosphorescence emission spectroscopy was also applied to clarify the photoactivation properties of silica-alumina. It is concluded that the highly dispersed and isolated tetrahedral AlO₄ species in silica matrix, which exhibit the fine structural phosphorescence spectra centred at 520 nm, would be the highly active sites for ethane formation. On the other hand, the aggregated Al oxide species would be the active sites for producing both ethane and ethene with low activity.

Introduction

In order to make an efficient utilization of natural gas, we must consider transforming it into more valuable chemicals. Higher hydrocarbons are more useful for chemical industry. The oxidative coupling of methane (OCM) is one of the effective reactions producing higher hydrocarbons and has been extensively studied worldwide over the past two decades. The OCM reaction has the thermodynamical advantage in comparison with the direct coupling reaction of methane without oxidant. However, no catalysts could reach the principal criteria for industrial application of OCM.¹ It is quite difficult to obtain the coupling products in high yield, because the oxidation of coupling products to CO_x proceeds more selectively than the coupling reaction. The limits of the process have been essentially indicated.² Developments of other processes are required.

Photoinduced reaction is one of the most available reactions. The system employing photoinduced reaction has some advantages: It works even at room temperature and it might employ solar energy so that it is environmentally benign. In addition, even the thermodynamically difficult reaction may possibly proceed in photoinduced system. Actually, several researchers have tried to activate methane by employing photoinduced system.

For example, photoinduced oxidative methane coupling system has already been investigated by using TiO₂ at 373–473 K in the presence of oxygen.³ However, the most important problem on this system was high selectivity to CO₂ in addition to low yield. To avoid complete oxidation, the photoinduced non-oxidative coupling systems without using oxidant molecules were examined by employing transition metal oxides, such as V/SiO₂,⁴ TiO₂⁵ and Mo/SiO₂.⁶ However, for example, in the system employing Mo/SiO₂, which

showed the highest yield among them, the product yield in the gaseous phase was low and heating or admission of water vapor were required to collect the adsorbed coupling products.⁶

Recent developments in the photocatalysis systems led us to recognize that the employment of transition metal oxides is not the sole solution. Some kinds of photoreactions were successively discovered on silica and silica-based materials, e.g., photoisomerization of butene,⁷ photometathesis of alkenes,^{8–12} photooxidation of alkenes,^{13–17} and photooxidation of CO.¹⁸ In addition, silica-alumina was found to exhibit a characteristic phosphorescence emission spectrum,¹⁹ which predicted that silica-alumina might function as a photocatalyst.

Recently, we have found out that the photoinduced non-oxidative coupling of methane proceeds on silica-alumina around room temperature.²⁰ In this system C₂₊ products are obtained in the gaseous phase without any forced desorption process, and no oxygenated products are formed, including CO_x. In addition, the stoichiometric formation of H₂ was also revealed.²¹ Hydrogen is being used as a fuel, and is thought to be a clean energy source for the twenty-first century to meet environmental requirements. This photoreaction is very attractive since this reaction is energetically up-hill type reaction ($\Delta G > 0$) where the total chemical potentials of products, such as ethane and hydrogen, are higher than that of reactant, methane:



This means that the photoenergy is partially stored as chemical potential in the products.

In the present work, we examined the activity on a series of sol–gel prepared silica-alumina samples containing

various aluminium contents and discuss the active sites on the silica-alumina for photoinduced non-oxidative methane coupling.

Experimental

Materials

The samples of silica-alumina were prepared by the sol-gel method.²² After a mixture of $\text{Si}(\text{OEt})_4$ and ethanol (mol ratio, 1/5) was stirred for 1 h, another mixture of ethanol, distilled water, $\text{Al}(\text{NO}_3)_3$ and nitric acid (mol ratio, 5/50/ x /0.02, $x = 0.02 - 2$) was added dropwise, followed by stirring for 1 h. Dehydration proceeded at 353 K with suction. When gelation started, the mixture was dried without stirring, followed by drying at 383 K for 12 h, grinding in air at room temperature and calcination in a flow of dry air (60 ml min^{-1}) at 773 K for 5 h to obtain the silica-alumina powder samples. The Al content (mol%) calculated from the amount of the reagents used was defined as a molar ratio of the number of Al atoms to the total number of Si and Al atoms in the silica-alumina; $N_{\text{Al}}/(N_{\text{Si}} + N_{\text{Al}}) \times 100$.

Pure silica sample was prepared from $\text{Si}(\text{OEt})_4$ by the sol-gel method in a water-ethanol mixture at boiling point followed by grind and calcination.²³ Pure alumina was prepared by calcination of $\text{Al}(\text{NO}_3)_3$. They were stored under *ca.* 80% humidity at room temperature.

Two reference samples were employed for Al K-edge XANES study.^{24,25} MFI-type aluminosilicate (JRC-Z5-25H,²⁶ $\text{SiO}_2/\text{Al}_2\text{O}_3 = 25$, known as H-ZSM-5) containing Al atoms in the zeolite framework, tetrahedral site, was supplied from the Catalysis Society of Japan. θ -Alumina, in which Al atoms are equally distributed between the tetrahedral and octahedral sites of spinel, was prepared by calcination of γ -alumina (JRC-ALO-4^{26,27} supplied from the Catalysis Society of Japan) at 1073 K for 12 h.

Methane (99.95%) was purified by a vacuum evaporation before every use.

Photoreaction test

The reaction test was carried out in a closed quartz reaction vessel (82 cm^3). The sample (1.0 g) was spread on the flat bottom of the vessel (19.6 cm^2). Before the reaction test, the sample was heated in air up to 1073 K and then evacuated. Subsequently the sample was treated with 60 Torr oxygen ($1 \text{ Torr} = 133.3 \text{ N m}^{-2}$) at 1073 K for 1 h, followed by evacuation at the same temperature for 1 h and then by introduction of methane at room temperature. The initial pressure of methane ($200 \text{ } \mu\text{mol}$) in the reactor was 45 Torr and no oxidant molecule was introduced into the reaction system. The sample was irradiated with a 250 W Xe lamp for 6 h. Under photoirradiation, the temperature of sample bed was measured to be *ca.* 310 K. Products in the gaseous phase were analyzed by GC. Then adsorbed products were thermally desorbed by heating (573 K , 15 min), collected, and analyzed.

Characterizations

Specific surface areas (BET) were calculated from N_2 -adsorption at 77 K. Powder X-ray diffraction (XRD) patterns were recorded on a Rigaku diffractometer RINT 1200 using a radiation of Ni-filtered $\text{Cu-K}\alpha$ radiation (40 kV, 20 mA). X-ray photoelectron spectra (XPS) were recorded with a Shimadzu ESCA-3300 spectrometer using $\text{Mg-K}\alpha$ radiation (10 kV, 20 mA, 1253.6 eV) to calculate surface concentrations of Al and Si estimated by the band area intensity of Al 2p and Si 2s, respectively.

Soft X-ray absorption experiments were carried out on the beam line 7A²⁸ at UVSOR, Institute for Molecular Science,

Okazaki, Japan, with ring energy 750 MeV and stored current of 130–200 mA. A two-crystal monochromator employing YB_{66} crystals²⁹ was used for recording Al K-edge XANES. Data were collected in a total electron yield mode under high vacuum (residual pressure $< 1 \times 10^{-6}$ Torr) at room temperature. The sample was put on the first Cu-Be dynode of the electron multiplier (-1.5 kV) by using an adhesive carbon tape.

Diffuse reflectance UV-vis spectra were recorded on a JASCO V-570 equipped with an integrating sphere covered with BaSO_4 . Phosphorescence spectra were recorded at 77 K with a Hitachi F-4500 fluorescence spectrophotometer using UV filter ($\lambda_{\text{transmittance}} > 330 \text{ nm}$) to remove scattered light from UV source (Xe lamp) and an attached apparatus to cut fluorescence. The excitation wavelength employed was 300 nm. Phosphorescence from the optical cell was weak enough to ignore in most cases. Before recording UV-visible absorption spectra and phosphorescence spectra, the sample (0.5 g) was treated with 60 Torr ($1 \text{ Torr} = 133 \text{ Pa}$) O_2 for 1 h at 1073 K in a pretreatment part of an *in situ* cell, followed by evacuation for 1 h at the same temperature. Then, the sample was transferred to the optical part without exposing to air.

Results

Structure of the silica-alumina samples

We prepared a series of silica-alumina containing 0–100% of Al. Table 1 shows the specific surface areas of the silica-alumina samples as synthesized (calcined) and those of the samples pretreated at 1073 K. All the samples had a specific surface area larger than $140 \text{ m}^2 \text{ g}^{-1}$ after calcination at 773 K. Even after pretreatment at 1073 K, the samples maintained a high surface area larger than $90 \text{ m}^2 \text{ g}^{-1}$. Although the pretreatment at high temperature reduced the specific surface area of the samples to some extent, high temperatures such as 1073 K were employed for the sample pretreatment in this study. This is because the yield of photoinduced methane coupling increased with an increase of the pretreatment temperature in spite of the decrease of specific surface area.²¹ It was suggested that surface dehydration was related to formation of the active sites.^{21,30}

The silica and the silica-alumina samples of lower than 50 mol% Al were basically amorphous structure as shown by XRD (Fig. 1(a)–(c)). Other phases such as alumina, zeolite and layered structures were not observed. As for the high Al sample of 66.7 mol% Al (Fig. 1(d)), broad diffraction lines were observed at 46° and 67° , which were assignable to bulk $\gamma\text{-Al}_2\text{O}_3$. The broadness of the diffraction means that the alu-

Table 1 Al contents and specific surface areas of the synthesized samples

Al content/mol% ^a	BET surface area/ $\text{m}^2 \text{ g}^{-1}$	
	As synthesized	After pretreatment at 1073 K
0.0 ^b	633	297
2.0	464	137
9.1	498	258
16.7	489	273
37.5	264	203
50.0	143	98
66.7	149	93
100 ^c	241	92

^a Al content (mol%) calculated from the amount of the reagents used was defined as a molar ratio of the number of Al atoms to the total number of Si and Al atoms in the silica-alumina; $N_{\text{Al}}/(N_{\text{Si}} + N_{\text{Al}}) \times 100$. ^b The silica sample. ^c The alumina sample.

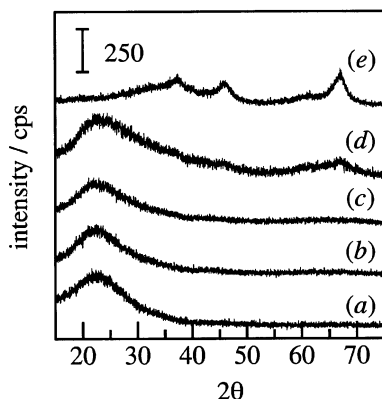


Fig. 1 XRD patterns of the silica sample (a), the silica-alumina samples whose Al contents (mol%) was 25.0 (b), 50.0 (c), 66.7 (d), and the alumina sample (e).

mina crystallites would have small size or low crystallinity. The alumina sample (Fig. 1(e)) showed the diffraction pattern assigned to γ - Al_2O_3 .

The Al composition at surface layers of the silica-alumina samples is estimated by XPS analysis and plotted as a function of the Al content (Fig. 2). A good linear correlation was obtained as shown, meaning that the Al ions/species were homogeneously dispersed on the surface and bulk of the silica. In the present paper, the Al content is employed as the Al surface composition.

Al K-edge XANES is useful to determine the aluminium coordinations (AlO_4 tetrahedra and AlO_6 octahedra) in oxide environments.^{24,25,31–34} Fig. 3 shows the normalized Al K-edge XANES spectra of the silica-alumina samples and the alumina samples used for the photoreaction (Fig. 3(a)–(g)), together with those of reference compounds. The white line peak at 1566 eV is assigned to the tetrahedral AlO_4 compounds, while the peaks at 1568 eV and at 1572 eV are assigned to octahedral AlO_6 compounds.^{31,32} However, since the peak at 1572 eV is not suitable for quantitative analysis,^{24,25} the peaks at 1566 eV and at 1568 eV are employed for the estimation of the fraction of the tetrahedral AlO_4 species and the octahedral AlO_6 species, respectively. The MFI-type zeolite having AlO_4 species shows a peak at 1566 eV (Fig. 3(h)), while the θ -alumina, which consists of the AlO_4 and AlO_6 species equally, shows almost the same intensity of peaks at 1566 eV and 1568 eV (Fig. 3(i)).^{24,25,35}

The spectra of the silica-alumina samples gradually varied with the Al content (Fig. 3(a)–(f)). This means that the local structure of Al species in silica-alumina gradually varied with the Al content. The low Al content samples of 2 and 9.1 mol% Al (Fig. 3(a), (b)) show a peak at around 1566 eV, which is assigned to the AlO_4 species. This peak was broadened to

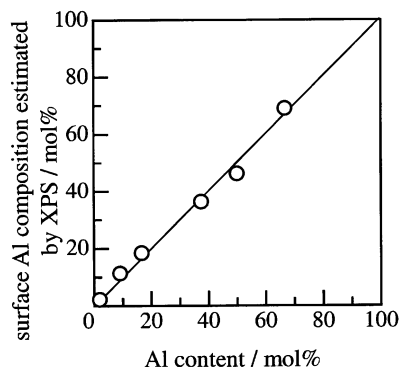


Fig. 2 Relationship between the surface Al composition estimated by XPS and the Al content calculated from the amount of reagents used.

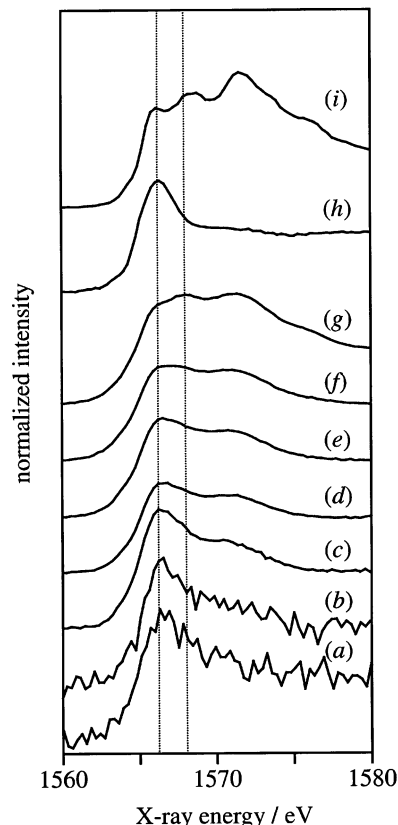


Fig. 3 Normalized Al K-edge XANES spectra of the silica-alumina samples used for the photoreaction, whose Al contents (mol%) was 2.0 (a), 9.1 (b), 16.7 (c), 37.5 (d), 50.0 (e), 66.7 (f), and those of the alumina sample used for the photoreaction (g), the MFI-type zeolite having AlO_4 (h) and θ -alumina which contains equal amount of AlO_4 and AlO_6 (i).

higher energy with an increase of Al content, which is probably due to the overlap of the band at 1568 eV (Fig. 3(c)–(f)). The sample of 16.7 mol% Al seems to have a very small fraction of AlO_6 species and a dominant fraction of AlO_4 (Fig. 3(c)), while the samples of higher Al content have larger fractions of AlO_6 (Fig. 3(d)–(f)). The alumina sample showed the obvious peak at 1568 eV (Fig. 3(g)) together with the shoulder at 1566 eV. By comparison with the spectra of θ -alumina, there are almost an even amount of AlO_4 and AlO_6 species.

Thus, the AlO_4 species are predominant in the lower Al content silica-alumina samples, and the fraction of the AlO_6 species in the silica-alumina samples increased gradually with an increase of Al content. In the high Al content samples and alumina sample, the amount of the AlO_4 species and the AlO_6 species are almost even.

Photoabsorption and phosphorescence of the silica-alumina samples

Fig. 4 shows the diffuse reflectance UV–vis spectra of the samples evacuated at 1073 K. All the silica-alumina samples showed the maximum absorbance around 230 nm and the intensity varied with Al content. The maximum absorption intensity around 230 nm was plotted in Fig. 5. The absorption intensity increased with an increase of Al content up to around 20 mol%, then gradually decreased. The intense photoabsorption should be related to a certain Si–O–Al sites in silica-alumina, since silica and alumina themselves exhibited low absorption as shown at 0% and 100% in Fig. 5, respectively.

It has been reported that the highly dispersed AlO_4 species in silica-alumina evacuated at high temperature such as 1073 K exhibit a characteristic fine structural phosphorescence spectrum.^{19,21,30} Fig. 6 shows the phosphorescence emission spectra

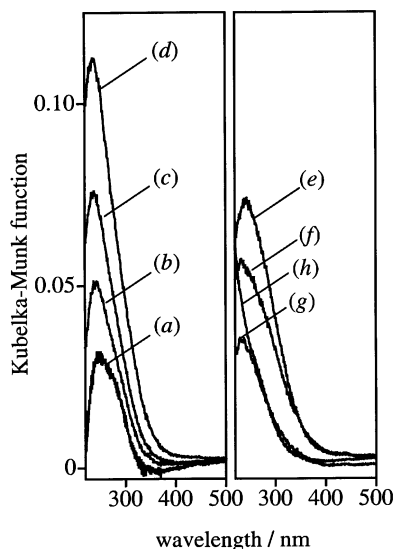


Fig. 4 Diffuse reflectance UV-vis spectra of the silica (a) and the silica-alumina samples whose Al content (mol%) was 2.0 (b), 9.1 (c), 16.7 (d), 37.5 (e), 50.0 (f), 66.7 (g), and that of the alumina sample (h). The samples were pretreated at 1073 K.

of the present samples evacuated at 1073 K. The intensity in Fig. 6 was normalized by each appropriate factor to discuss the line shape. The pure silica exhibited a broad band with a maximum around 460 nm (Fig. 6(a)). On the spectra of the silica-alumina samples of 2.0–37.5 mol% Al (Fig. 6(b)–(e)), the fine structure was clearly observed as reported, indicating that there are highly dispersed AlO_4 species existing in the silica matrix. The progressions show that photoexcitation occurs a certain localized site, probably due to vibration of M–O (M = Al or Si) moiety related to AlO_4 species. As the Al content increases further, the fine structure became unclear, and finally the alumina sample showed a broad band centered around 470–480 nm (Fig. 6(h)). The spectra of the high Al content samples (Fig. 6(f) and 6(g)) resemble that of the alumina sample (Fig. 6(h)).

The phosphorescence intensity (at 520 nm) of the samples was plotted in Fig. 7. Among all samples, the four silica-alumina samples of low Al content (2.0–37.5 mol% Al) showed high intensity with the fine structure, and the maximum is around 20 mol% Al.

Photoinduced methane coupling activity of the silica-alumina samples

All these prepared samples, silica, silica-alumina and alumina, exhibited activity for the photoinduced non-oxidative methane

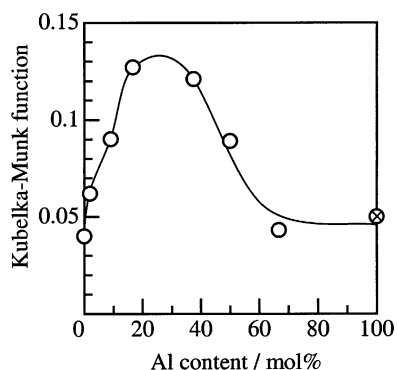


Fig. 5 The maximum absorption intensity around 230 nm in the diffuse reflectance UV-vis spectra shown in Fig. 4. As for the alumina sample (the point of 100 mol%), the intensity at 230 nm was employed.

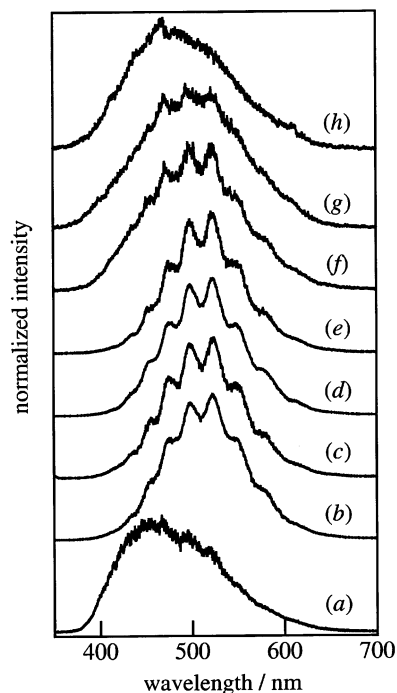


Fig. 6 Normalized phosphorescence spectra of the silica sample (a), the silica-alumina samples whose Al contents (mol%) was 2.0 (b), 9.1 (c), 16.7 (d), 37.5 (e), 50.0 (f), 66.7 (g), and the alumina sample (h) measured at 77 K. The excitation wavelength was 300 nm. The samples were pretreated at 1073 K.

coupling around room temperature. Only ethane was obtained as the gaseous product under this condition, except for the sample of 16.7 mol% Al; on the 16.7 mol% Al silica-alumina sample which showed the maximum conversion, a trace amount of propane was also produced. Ethene was detected as a thermally desorption product on some samples of high Al contents. Molecular hydrogen was produced stoichiometrically within experimental error in this system, as reported elsewhere.²¹

The yields of ethane and adsorbed ethene are shown in Fig. 8(a) and 8(b) as a function of the Al content. The reproducibility was confirmed on some representative points. The curve for the ethane yield (Fig. 8(a)) shows a maximum at around 20 mol% Al. Note that the curve showing the ethane yield in Fig. 8(a) resembles the curves showing the photoabsorption intensity in Fig. 5 and the phosphorescence intensity of the samples below 20 mol% Al in Fig. 7. On the other hand, the ethene yield increased with Al content, especially over 20 mol% (Fig. 8(b)). The selectivity to ethane (Fig. 8(c)) was *ca.* 100% on the silica and silica-alumina samples below 20

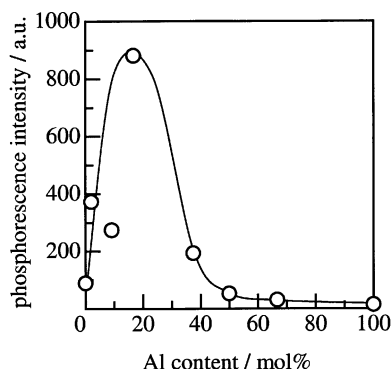


Fig. 7 The phosphorescence intensity at 520 nm of the samples evacuated at 1073 K. The excitation wavelength was 300 nm.

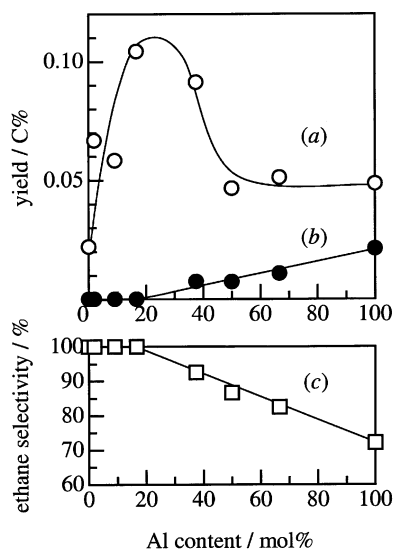


Fig. 8 The yield of ethane (a) and adsorbed ethene (b), and the ethane selectivity (c) in photoinduced non-oxidative methane coupling over a series of the silica sample, the silica-alumina samples and the alumina sample.

mol% Al content, and decreased almost linearly with increasing Al content over 20 mol% Al. On the alumina sample, the selectivity was *ca.* 70%.

Discussion

Structural aspects of the aluminium species in silica-alumina

The silica-alumina samples below 50 mol% Al showed similar XRD patterns to silica but no diffraction lines due to alumina (Fig. 1(a)–(c)). With low Al content samples (2.0 and 9.1 mol%), XANES spectra indicate that the dominant aluminium species were coordinated by four oxygen atoms (Fig. 3). Both samples of 2.0 and 9.1 mol% Al showed the fine structural phosphorescence spectra due to highly dispersed AlO_4 species (Fig. 6). These results indicate that the major aluminium species in these low Al silica-alumina samples were highly dispersed AlO_4 species. The proposed model is shown in Fig. 9(a). The highly dispersed AlO_4 species are proposed to be isolated in the SiO_4 tetrahedra network, or, in other words, they are surrounded by SiO_4 species as the first neighbor tetrahedral units. When Al content is low, the aluminium would

atomically substitute for silicon in silica tetrahedra network, and the Al species should be AlO_4 tetrahedra.

On the other hand, when the aluminium content increases, the AlO_4 species could no longer be isolated and small Al oxide clusters and alumina crystallites that consist of both AlO_4 and AlO_6 should be also formed in the sample. It is supposed that this variation of Al species in the silica-alumina occurs monotonously with the increasing of the Al content. Judging from XANES spectrum (Fig. 3(c)), a very small fraction of AlO_6 that most probably belongs to small Al oxide clusters seemed to exist in the 16.7 mol% Al sample. However, it would be recognized that the major species are still the highly dispersed AlO_4 species. The sample of 16.7 mol% Al exhibited the maximum intensity on the phosphorescence emission spectra with the fine structure (Figs. 6 and 7). This means that there is the maximum amount of the highly dispersed AlO_4 species among the series of the silica-alumina samples. The illustrated model of this state is proposed in Fig. 9(b) though small Al oxide cluster species in silica matrix as a very minor species are not shown here.

As for the sample of 37.5 mol% Al, XANES spectrum (Fig. 3(d)) indicated the existence of both AlO_4 and AlO_6 species more clearly than that of the lower Al content samples, while the phosphorescence spectrum (Fig. 6) showed that a small fraction of highly dispersed AlO_4 species still exists. On the 37.5 mol% Al sample, it is suggested that a small fraction of highly dispersed AlO_4 species coexist with small Al oxide clusters consisting of AlO_4 and AlO_6 as shown in Fig. 9(c).

On the high Al content samples such as 50 and 66.7 mol% Al, the fraction of the AlO_6 species became larger as clarified by XANES spectra (Fig. 3(e) and 3(f)). Moreover, in these samples, the line shapes of the phosphorescence spectra (Fig. 6(f) and 6(g)) were different from that of the low Al sample, but resemble rather that of alumina (Fig. 6(h)), and the phosphorescence intensity was very low (Fig. 7). These findings support the idea that the more aggregated Al oxide species such as alumina crystallites became the major species in these samples at the sacrifice of the highly dispersed AlO_4 species and small Al oxide clusters. In the case of the 66.7 mol% Al sample, the γ -alumina phase was detected by XRD (Fig. 3), confirming that the alumina crystallites exist; this sample would contain a larger amount/size of crystallites than the sample of 50.0 mol% Al.

As a conclusion about the structure of the silica-alumina samples, the variation in the amount of each Al species with increasing the Al contents is summarized here. The amount of the highly dispersed AlO_4 species increased with an increase of the Al content to reach a maximum in the sample of around 20 mol% Al, then decreased. The amount of small Al oxide

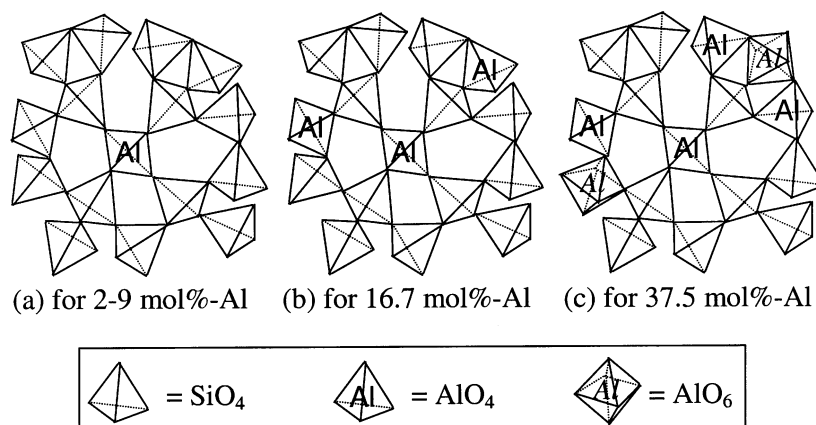


Fig. 9 Tentatively proposed models for some major AlO_4 species in the silica-alumina samples of 2 and 9 mol% Al (a), 16.7 mol% Al (b), and 37.5 mol% Al (c). Highly dispersed AlO_4 species are in the silica-alumina samples less than 16.7 mol% Al, while small Al oxide clusters consisting of AlO_4 and AlO_6 exist in the high Al content samples.

clusters also gradually increased at least from around 20 mol% Al at the sacrifice of the highly dispersed AlO_4 species. Then, in the high Al content samples, the highly dispersed AlO_4 species decreased further while the Al oxide clusters and crystallites became major. In this way, although the variation of the species should be monotonous, the amount of the highly dispersed species shows a maximum, and then decreases with increasing the Al content.

The photoabsorption and photoreaction activity of alumina species

For the photoinduced reaction, photoexcitation is the essential process. Though methane molecules absorb light in the vacuum-UV region, such as 94, 120 and 128 nm wavelength, they cannot absorb the light in the region of ultraviolet and visible light that come from the Xe-lamp through air. Without the silica-alumina samples, methane could not be converted even upon photoirradiation. As mentioned above, the silica-alumina samples showed a photoabsorption band in the UV region around 230 nm (Fig. 4), and the variation of the photoabsorption intensity with the Al content (Fig. 5) was in good agreement with the activity for the photoinduced non-oxidative methane coupling (Fig. 8(a)). These findings strongly suggest that the surface photoabsorption sites on the silica-alumina would first absorb the light around 230 nm to be excited, and then would transfer the energy to the adsorbed methane molecule.

The pure silica (0 mol% Al) also exhibited activity for this reaction. As mentioned above, the pure silica materials have been reported to promote some photoinduced reactions.^{8–14} In those cases, the surface defects or surface activated sites on silica are thought to be the active sites. Also in the photoinduced non-oxidative methane coupling, these surface sites might be active sites when there is no aluminium in the sample. However, the activities on all silica-alumina samples were higher than the pure silica. Thus, it is suggested that the major active sites on silica-alumina are aluminium-related sites. Assuming that only the Al sites are the active sites on silica-alumina, the relative specific activity was estimated: The product yield per hour was divided by the BET specific surface area and by the Al composition. The values for ethane and adsorbed ethene were plotted in Fig. 10. Here, although the silica-alumina sample of 2 mol% Al (the plot for ethane was not shown) showed too high a value alone (8 times larger than the sample of 9.1 mol% Al), it might be overestimated because

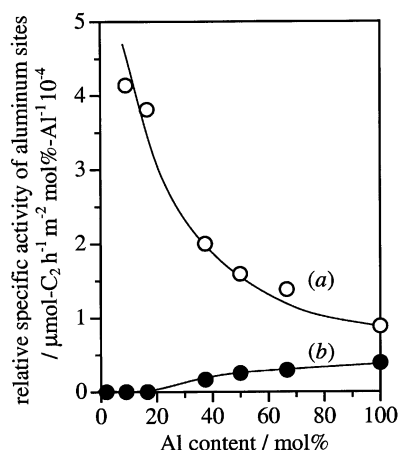


Fig. 10 The relative specific activity of aluminium sites for the formation of ethane (a) and ethene (b) in photoinduced non-oxidative methane coupling over a series of the silica-alumina samples. The relative specific activity is the yield per hour normalized by the specific surface area and the Al composition. The plot of the sample of 2 mol% Al for ethane was eliminated (see text).

of existence of other active sites on the silica surface. Fig. 10 shows that the average specific activity of the Al sites in silica-alumina samples decreased obviously with an increase of the Al content. This means that the decrease of the product yield on the samples of higher Al content than 20% Al would not be only due to the decrease in the surface area but also due to the decrease in the average specific activity of each Al sites.

In addition to this variation of the average specific activity of the Al sites (Fig. 10), the ethane yield showed the maximum around 20 mol% Al, then decreased with increasing the Al content (Fig. 8(a)), while the selectivity of ethane also started to decrease around 20 mol% Al (Fig. 8(c)). These variations on the activity would be explained by the amount and performance of the representative two Al species; one is the highly dispersed AlO_4 species (Fig. 9(a), 9(b)) and another is the aggregated Al oxide species (major species in Fig. 9(c)).

The silica-alumina samples of low Al content less than 16.7 mol% have predominantly the highly dispersed AlO_4 species. In the qualitative view, the highly dispersed AlO_4 species exhibited high specific activity per surface aluminium (Fig. 10(a)) and high ethane selectivity (Fig. 8(c)). In the quantitative view, the sample of 16.7 mol% Al, which has the largest amount of this species, exhibited the highest ethane yield (Fig. 8(a)) and the most intense UV absorption band (Fig. 4(b)–(d)). Thus the highly dispersed AlO_4 species are effectively excited by UV light and exhibit the high activity for the selective ethane formation.

The highly dispersed AlO_4 species exhibited fine structural phosphorescence spectra when they were excited by UV light. The properties of these photoexcited sites were well studied by monitoring the phosphorescence emission spectra,³⁰ and it was clarified that the photoexcited sites could activate the methane molecules.²¹ In the present study, a good correlation was revealed between the phosphorescence intensity and the photoactivity for this reaction among the low Al content samples less than 20 mol%. This strongly supports that the phosphorescence sites act as the highly active sites for ethane formation.

As the Al content increased to more than 50 mol% Al, the product selectivity for ethane decreased, and the formation of adsorbed ethene increased, as shown in Fig. 8. This would correspond to the formation of the small Al oxide clusters and crystallites (AlO_4 and AlO_6 species). Thus, it is demonstrated that these aggregated species, such as the Al oxide clusters and crystallites, in silica-alumina produce both ethane and ethene.

Although the aggregated alumina species such as clusters and crystallites also absorbed photoenergy and actually promoted the coupling of methane, the weak phosphorescence spectra without the fine structure were clearly different from those of the highly dispersed Al species. The aggregated Al species would activate methane molecules upon photoirradiation by a different photoexcitation mechanism to those on the highly dispersed AlO_4 species, resulting in the formation of both ethane and ethene.

Conclusion

The silica-alumina samples in the entire range of Al concentration exhibit the activity for the photoinduced non-oxidative methane coupling. The highly dispersed AlO_4 species, which are dominant in the low Al silica-alumina samples and exhibit the fine structural phosphorescence spectra, are the highly active sites for the selective ethane production. On the other hand, the aggregated Al oxide species such as Al oxide clusters and crystallites, which are major in the high Al silica-alumina, are the active sites for the formation of both ethane and ethene.

Acknowledgement

The authors thank Professor Atsushi Satsuma for valuable discussions. Dr Ken-ichi Shimizu and Dr Tomoko Yoshida are acknowledged for their cooperation on the XAFS measurements. X-ray absorption experiments were carried out as the Joint Studies Program (1997) of UVSOR of the Institute for Molecular Science. H. Y. acknowledges the Nippon Sheet Glass Foundation for Materials Science and Engineering, The Nitto Foundation, and Japan Chemical Innovation Institute (JCII) for the financial support. This work was also supported by a grant-in-aid for Exploratory Research from the Ministry of Education, Culture, Sports, Science and Technology (MEXT), Japan.

References

- 1 Y. Xu and L. Lin, *Appl. Catal. A*, 1999, **188**, 53.
- 2 H. D. Gesser and N. R. Hunter, *Catal. Today*, 1998, **42**, 183 and references therein.
- 3 K. Okabe, K. Sayama, H. Kusama and H. Arakawa, *Chem. Lett.*, 1997, 457.
- 4 S. L. Kaliaguine, B. N. Shelimov and V. B. Kazansky, *J. Catal.*, 1978, **55**, 384.
- 5 G. N. Kuzmin, M. V. Knatko and S. V. Kurganov, *React Kinet. Catal. Lett.*, 1983, **23**, 313.
- 6 W. Hill, B. N. Shelimov and V. B. Kazansky, *J. Chem. Soc., Faraday Trans. 1*, 1987, **83**, 2381.
- 7 A. Morikawa, M. Hattori, K. Yagi and K. Otsuka, *Z. Phys. Chem., N. F.*, 1977, **140**, 309.
- 8 H. Yoshida, T. Tanaka, S. Matsuo, T. Funabiki and S. Yoshida, *J. Chem. Soc., Chem. Commun.*, 1995, 761.
- 9 T. Tanaka, S. Matsuo, T. Maeda, H. Yoshida, T. Funabiki and S. Yoshida, *Appl. Surf. Sci.*, 1997, **121/122**, 296.
- 10 H. Yoshida, K. Kimura, Y. Inaki and T. Hattori, *Chem. Commun.*, 1997, 129.
- 11 Y. Inaki, H. Yoshida, K. Kimura, S. Inagaki, Y. Fukushima and T. Hattori, *Phys. Chem. Chem. Phys.*, 2000, **2**, 5293.
- 12 Y. Inaki, H. Yoshida and T. Hattori, *J. Phys. Chem. B*, 2000, **104**, 10304.
- 13 H. Yoshida, T. Tanaka, M. Yamamoto, T. Funabiki and S. Yoshida, *Chem. Commun.*, 1996, 2125.
- 14 H. Yoshida, T. Tanaka, M. Yamamoto, T. Yoshida, T. Funabiki and S. Yoshida, *J. Catal.*, 1997, **171**, 351.
- 15 M. Anpo, C. Yun and K. Kubokawa, *J. Catal.*, 1980, **61**, 267.
- 16 Y. Kubokawa, M. Anpo and C. Yun, *Proc. 7th Int. Congress Catal. (B)*, 1980, 1171.
- 17 H. Yoshida, C. Murata, Y. Inaki and T. Hattori, *Chem. Lett.*, 1998, 1121.
- 18 A. Ogata, A. Kazukawa and M. Enyo, *J. Phys. Chem.*, 1986, **90**, 5201.
- 19 H. Yoshida, T. Tanaka, A. Satsuma, T. Hattori, T. Funabiki and S. Yoshida, *Chem. Commun.*, 1996, 1153.
- 20 Y. Kato, H. Yoshida and T. Hattori, *Chem. Commun.*, 1998, 2389.
- 21 H. Yoshida, Y. Kato and T. Hattori, *Stud. Surf. Sci. Catal.*, 2000, **130**, 659.
- 22 M. Taira and M. Yamaki, *J. Mater. Sci.: Mater. Med.*, 1995, **6**, 197.
- 23 H. Yoshida, C. Murata and T. Hattori, *J. Catal.*, 2000, **194**, 364.
- 24 K. Shimizu, Y. Kato, T. Yoshida, H. Yoshida, A. Satsuma and T. Hattori, *Chem. Commun.*, 1999, 1681.
- 25 Y. Kato, K. Shimizu, N. Matsushita, T. Yoshida, H. Yoshida, A. Satsuma and T. Hattori, *Phys. Chem. Chem. Phys.*, 2001, **3**, 1925.
- 26 T. Uchijima, *Catalytic Science and Technology*, ed. S. Yoshida, N. Takazawa and Y. Ono, Kodansha, VCH, Tokyo, 1991, vol. 1, p. 393.
- 27 Y. Murakami, *Stud. Surf. Sci. Catal.*, 1983, **16**, 775.
- 28 T. Murata, T. Matsukawa, S. Naoe, T. Horigome, O. Matsudo and M. Watanabe, *Rev. Sci. Instrum.*, 1992, **63**, 1309.
- 29 T. Kinoshita, Y. Takata, T. Matsukawa, H. Aritani, S. Matsuo, T. Yamamoto, M. Takahashi, H. Yoshida, T. Yoshida, Y. Ufuketepe, K. G. Nath, S. Kimura, H. Kumigashira and Y. Kitajima, *J. Synchrotron Rad.*, 1998, **5**, 726.
- 30 Y. Kato, H. Yoshida and T. Hattori, *Phys. Chem. Chem. Phys.*, 2000, **2**, 4231.
- 31 D. A. McKeown, G. A. Waychunas and G. E. Brown, Jr., *J. Non-Cryst. Solids*, 1985, **74**, 349.
- 32 D. Cabaret, P. Sainctavit, P. Ildelfonse and A.-M. Flank, *J. Phys.: Condens. Matter*, 1996, **8**, 3691.
- 33 M. Fröba and M. Tiemann, *Chem. Mater.*, 1998, **10**, 3475.
- 34 J. A. van Bokhoven, H. Sambe, D. E. Ramaker and D. C. Koningsberger, *J. Phys. Chem. B*, 1999, **103**, 7557.
- 35 Although the peak height at 1568 eV seems larger than that at 1566 eV, it is mainly due to the overlapping of the continuum absorption of AlO₄ species that appears at lower energy.